Photoelectron emission from LiF surfaces by ultrashort electromagnetic pulses

M. A. Acuña[1] and M. S. Gravielle[1,2]

[1]*Instituto de Astronomía y Física del Espacio, Consejo Nacional de Investigaciones Científicas y Técnicas, Universidad de Buenos Aires, Buenos Aires, Argentina*

[2]*Departamento de Física, Facultad de Ciencias Exactas y Naturales, Universidad de Buenos Aires, Argentina*

(Received 9 September 2010; revised manuscript received 26 January 2011; published 30 March 2011)

Energy- and angle-resolved electron emission spectra produced by incidence of ultrashort electromagnetic pulses on a LiF(001) surface are studied by employing a distorted-wave method named the crystal surface–Volkov (CSV) approximation. The theory makes use of the Volkov phase to describe the action of the external electric field on the emitted electron, while the electron-surface interaction is represented within the tight-binding model. The CSV approach is applied to investigate the effects introduced by the crystal lattice when the electric field is oriented parallel to the surface plane. These effects are essentially governed by the vector potential of the external field, while the influence of the crystal orientation was found to be negligible.

DOI: 10.1103/PhysRevA.83.032904 PACS number(s): 79.20.Ds, 79.60.−i, 78.47.J−, 42.65.Re

I. INTRODUCTION

Recent improvements on attosecond laser-pulse technologies have renewed interest in the interaction of electromagnetic fields with surfaces [1–4]. In particular, pump-probe experiments of photoemission from metal surfaces [5–7] are opening the way to study the dynamics of electrons in condensed matter in real-time [8,9]. In these experiments emitted electrons come from two different sources: the conduction band and the core levels. While electrons coming from the conduction band are initially bound to the surface in delocalized states, being able to move almost freely inside the solid, core electrons originate from the inner shells of solid atoms, being initially concentrated around target nucleus. The aim of this work is to study this last contribution separately by considering photoelectron emission from an insulator surface, like LiF. This material is a typical broad-band-gap solid with a narrow valence band, which indicates that all electrons are mainly localized around crystal ions, retaining essential parts of their atomic character.

Electron emission induced by the incidence of an ultrashort electromagnetic pulse on a LiF(001) surface is here described within a time-dependent distorted-wave theory, named the crystal surface-Volkov (CSV) approximation. The method is based on use of the Volkov phase [10] to represent the interaction of the active electron with the external field. This kind of one-active-electron theory has been recently applied to study different laser-induced electron emission processes from metal surfaces, providing reasonable predictions [11–14].

Due to the localized character of the electrons of the solid, the initial unperturbed state is represented by means of the tight-binding model [15], while in the final channel we also include the distortion produced by the charge imbalance originated by ionization, which can last for a period of time longer than the duration of the ultrashort pulse [16,17].

In this article we use the CSV approach to evaluate double-differential-energy and angular-electron distributions produced by few-cycle electromagnetic pulses that are linearly polarized along a direction parallel to the surface. Our purpose is to study the interference effects due to the crystal lattice in a way similar to that observed in the photoionization of molecules [18–20]. In order to analyze the influence of the surface on electron spectra, we compare the results to values derived from the atomic case, where only one target atom is considered.

The paper is organized as follows. In Sec. II we present the theory, in Sec. III results are shown and discussed, and finally in Sec. IV our conclusions are summarized. Atomic units are used throughout unless otherwise stated.

II. THEORETICAL MODEL

When a laser pulse impinges on an insulator surface (S), as a consequence of the interaction with the external field, an electron (e) of the solid, initially in a state ϕ_i with energy ε_i, can be ejected to the vacuum zone, ending in a final state ϕ_f with momentum $\vec{k}_f$ and energy $\varepsilon_f = k_f^2/2$. The temporal evolution of the electronic state $\Psi(\vec{r},t)$ associated with this process is determined by the time-dependent Schrödinger equation:

$$i\frac{\partial \Psi(\vec{r},t)}{\partial t} = [H_S + V_L(\vec{r},t)]\Psi(\vec{r},t), \tag{1}$$

where $\vec{r}$ is the position vector of the active electron e, $H_S = -\nabla_{\vec{r}}^2/2 + V_S$ is the unperturbed Hamiltonian, with V_S the electron-surface potential, and $V_L(\vec{r},t) = \vec{r}\cdot\vec{F}(t)$ is the interaction potential with the laser field $\vec{F}(t)$, expressed in the length gauge. The frame of reference is placed on a target nucleus belonging to the first atomic layer, with the $\hat{z}$ vector perpendicular to the surface plane, and the $\hat{x}$ and $\hat{y}$ vectors coinciding with the lattice axis.

We consider a linear polarized electric field $\vec{F}(t)$, whose temporal profile is defined as

$$F(t) = F_0 \sin(\omega t + \varphi)\sin^2(\pi t/\tau) \tag{2}$$

for $0 < t < \tau$ and 0 elsewhere, where τ determines the duration of the pulse, F_0 is the maximum field strength,

ω is the photon energy, and the phase φ is selected to be $\varphi = -\omega\tau/2 + \pi/2$ for a symmetric pulse.

In ionic insulator surfaces, as electrons are strongly localized around the ionic centers, we can employ the tight-binding model [15] to represent the initial unperturbed state $\phi_i(\vec{r},t) = \phi_i(\vec{r})\exp(-i\varepsilon_i t)$. The state $\phi_i(\vec{r})$, eigenfunction of H_S with energy ε_i, reads

$$\phi_i(\vec{r}) = \sum_{\vec{R}} e^{i\vec{K}\cdot\vec{R}}\,\varphi_i(\vec{r}-\vec{R}), \tag{3}$$

where the wave vector $\vec{K}$ has been introduced to identify a given crystal state within the surface band i, with $\vec{K}$ belonging to the first Brillouin zone. In Eq. (3) the function $\varphi_i(\vec{r}-\vec{R})$ represents the Wannier function centered on the lattice site $\vec{R}$ and the sum involves all $\vec{R}$ positions of the target ions. Since the overlap between wave functions corresponding to nearest-neighbor atoms is small, we approximate the Wannier function φ_i to the atomic wave function. As a rough estimation, the Bloch energy ε_i, corresponding to ϕ_i, can be expressed as [15]

$$\varepsilon_i \simeq \epsilon_i^{(at)} - \frac{\delta_i}{2}[\cos(K_x d_x)\cos(K_y d_y) + \cos(K_x d_x)\cos(K_z d_z) + \cos(K_y d_y)\cos(K_z d_z)], \tag{4}$$

where $\epsilon_i^{(at)}$ is the eigenenergy associated with the atomic state φ_i, δ_i is the bandwidth, and the distances d_x, d_y, and d_z are the shortest interatomic distances in the directions $\hat{x}$, $\hat{y}$, and $\hat{z}$, respectively.

A. CSV transition amplitude

Within the framework of the distorted-wave formalism, it is possible to derive an approximate solution of Eq. (1) by using the Volkov phase. The Volkov wave function represents the exact solution for a free electron moving in a time-dependent electric field [10], and its phase has been successfully employed for the description of atomic [21–25] and surface processes [13,26,27]. Making use of the well-known impulse approach [28,29], we propose a final distorted state that we call a CSV wave function, which reads

$$\chi_f^{(CSV)-}(\vec{r},t) = \phi_f(\vec{r})\exp[iD_L^-(\vec{k}_f,\vec{r},t) - i\varepsilon_f\, t], \tag{5}$$

where the minus sign indicates the incoming asymptotic condition and

$$\phi_f(\vec{r}) = \frac{\exp(i\vec{k}_f\cdot\vec{r})}{(2\pi)^{3/2}}\mathcal{D}_S^-(\vec{k}_f,\vec{r}) \tag{6}$$

represents the final unperturbed state, eigenfunction of H_S with with energy ε_f, with $\mathcal{D}_S^-(\vec{k}_f,\vec{r})$ the distortion introduced by the surface in the exit channel. In Eq. (5) the Volkov phase corresponding to the laser pulse,

$$D_L^-(\vec{k}_f,\vec{r},t) = \vec{A}^-(t)\cdot\vec{r} - \beta^-(t) - \vec{k}_f\cdot\vec{\alpha}^-(t), \tag{7}$$

is expressed in terms of the functions

$$\vec{A}^-(t) = -\int_{+\infty}^{t} dt'\vec{F}(t'),$$
$$\beta^-(t) = \frac{1}{2}\int_{+\infty}^{t} dt'[\vec{A}^-(t')]^2, \tag{8}$$
$$\vec{\alpha}^-(t) = \int_{+\infty}^{t} dt'\vec{A}^-(t'),$$

which are related to the vector potential (multiplied by the light velocity), the ponderomotive energy, and the quiver amplitude, respectively. Note that the distorted wave function given by Eq. (5) satisfies the proper asymptotic condition, *i.e.*, $\chi_f^{(CSV)-}(\vec{r},t) \to \phi_f(\vec{r})\exp(-i\varepsilon_f\, t)$ as $t \to +\infty$.

By using $\chi_f^{(CSV)-}$ within the *post* form of the first-order time-dependent distorted-wave theory [30], the CSV transition amplitude reads

$$T_{if}^{(CSV)} = a_{if} - i\int_{-\infty}^{+\infty} dt\langle\chi_f^{(CSV)-}(t)|W_f^\dagger(t)|\phi_i(t)\rangle, \tag{9}$$

where

$$a_{if} = \lim_{t\to-\infty}\langle\chi_f^{(CSV)-}(t)|\phi_i(t)\rangle \tag{10}$$

corresponds to the sudden amplitude that describes a sudden momentum transfer, while $W_f(t)$ denotes the final distortion potential, obtained from $W_f(t)|\chi_f^{(CSV)-}(t)\rangle = [H_S + V_L(\vec{r},t) - i\ d/dt]|\chi_f^{(CSV)-}(t)\rangle$. Replacing the initial unperturbed state given by Eq. (3) in Eq. (9) and taking into account that the electric field $F(t)$ vanishes outside the temporal interval $[0,\tau]$, $T_{if}^{(CSV)}$ can be expressed as

$$T_{if}^{(CSV)} = \sum_{\vec{R}} e^{i\vec{K}\cdot\vec{R}}\mathcal{A}_{if}(\vec{R}), \tag{11}$$

where

$$\mathcal{A}_{if}(\vec{R}) = \langle\chi_f^{(CSV)-}(0)|\varphi_i(0)\rangle - i\int_0^\tau dt\langle\chi_f^{(CSV)-}(t)|W_f^\dagger(t)|\varphi_i(t)\rangle \tag{12}$$

is the *partial* transition amplitude associated with electron emission from the atomic state $\varphi_i(\vec{r}_a,t) = \varphi_i(\vec{r}_a)\exp(-i\varepsilon_i t)$, which is centered on the position $\vec{R}$ of the lattice, with $\vec{r}_a = \vec{r} - \vec{R}$.

From Eq. (11) it is possible to interpret the process as a collection of individual transitions from different lattice sites $\vec{R}$. We assume that when the electron e is ionized from a region close to the $\vec{R}$ site, the charge of passive electrons fully screens the other ionic centers, but the hole left by the emitted electron is not instantaneously filled up as in metals, remaining in the exit channel [31]. Note that this effect is similar to the one giving rise to the track potential in the case of electron emission by projectile impact [16,32,33]. The hole-electron interaction is here represented by means of a Coulomb potential with an effective charge z_T. In addition, we neglect the effect of the response of the medium to the outgoing electron, which is weak in comparison with the hole potential [34]. Hence, in every term $\mathcal{A}_{if}(\vec{R})$ the function $\mathcal{D}_S^-(\vec{k}_f,\vec{r})$, included in Eq. (6), can be replaced by the

Coulomb distortion factor $D_T^-(\vec{k}_f,\vec{r}_a)=\exp[\pi z_T/(2k_f)]\Gamma(1+iz_T/k_f)_1F_1(-iz_T/k_f,1,-ik_f\ r_a-i\vec{k}_f\cdot\vec{r}_a)$, with ${}_1F_1$ the confluent hypergeometric function. Under this assumption, after some steps of algebra the transition amplitude $T_{if}^{(CSV)}$ reads

$$T_{if}^{(CSV)} = S_f(0)\left\langle\chi_f^{(at)-}(0)|\varphi_i(0)\right\rangle - i\int_0^\tau dt\, S_f(t)\left\langle\chi_f^{(at)-}(t)\right|\mathcal{W}_f^\dagger(t)|\varphi_i(t)\rangle\,, \qquad (13)$$

where

$$\chi_f^{(at)-}(\vec{r}_a,t) = \varphi_f(\vec{r}_a)\exp[iD_L^-(\vec{k}_f,\vec{r}_a,t) - i\varepsilon_f\ t] \qquad (14)$$

is the usual Coulomb-Volkov wave function associated with the atomic continuum state $\varphi_f(\vec{r}_a)=(2\pi)^{-3/2}\exp(i\vec{k}_f\cdot\vec{r}_a)\ D_T^-(\vec{k}_f,\vec{r}_a)$, and $\mathcal{W}_f(t)$ is the corresponding distortion potential [22]. In Eq. (13), the function $S_f(t)$ involves the crystallographic structure of the surface, reading

$$S_f(t) = \sum_{\vec{R}}\exp[i\vec{\Delta}_f(t)\cdot\vec{R}], \qquad (15)$$

where $\vec{\Delta}_f(t)=\vec{K}-\vec{k}_f-\vec{A}^-(t)$ is associated with the electron momentum transfer at the time t. Notice that if the function $S_f(t)$ is fixed as 1, $T_{if}^{(CSV)}$ coincides with the atomic transition amplitude evaluated within the Coulomb-Volkov approximation [22,25], except for the initial energy ε_i that is given by Eq. (4).

III. RESULTS

We apply the CSV approximation to study electron distributions produced by normal incidence of ultrashort and intense electromagnetic pulses on a LiF(001) surface. The LiF can be considered as the typical example of orthorhombic ionic crystal: valence electrons are localized around ionic centers, placed at sites of a fcc lattice, with $d_j = 3.8$ atomic units (a.u.) for $j = x,y,z$.

In this work we consider a field strength $F_0 = 0.01$ a.u., which, albeit intense, is lower than the damage threshold [7,35,36]. Under these conditions, the contribution of ionization from the K shell of Li^+ cations was found negligible and electrons emitted from the surface come mainly from the L shell of F^- anions. The wave functions φ_i corresponding to the different subshells of the negative fluor ion were represented by Hartree-Fock wave functions for negative ions [37], and no correction was included in φ_i to take into account the interaction of the target anion with nearest neighbors. The effective hole charge was chosen as $z_T = n_i\ (-2\epsilon_i^{(at)})^{1/2}$ [31,38], where n_i is the principal quantum number of the atomic state φ_i. The $2s$- and $2p$- bandwidths of fluor were estimated as 1.6 and 5.0 eV, respectively [39]. In our model we have not included the contribution of the dynamic electronic polarizability of the medium, which, although it is smaller for insulator materials than for metals, might be important for frequencies of the laser field resonant with the surface plasmon frequency ($\omega_S = 0.6$ a.u.).

For a given initial band i, the differential probability of electron emission is expressed in terms of the transition amplitude $T_{if}^{(CVS)}$, given by Eq. (13), as:

$$\frac{dP_i}{d\varepsilon_f d\Omega_f} = \rho_e\, k_f \int_{\mathcal{V}_B}\frac{d\vec{K}}{\mathcal{V}_B}\left|T_{if}^{(CSV)}\right|^2, \qquad (16)$$

where $\rho_e = 2$ is associated with spin states, Ω_f denotes the solid angle determined by $\vec{k}_f$, and the integration on the crystal vector $\vec{K}$ is made over the first Brillouin zone $\mathcal{V}_B$ [15]. Note that even though the $\vec{K}$ dependence has not been explicitly included, the integrand of Eq. (16) depends on $\vec{K}$ through the transferred momentum $\vec{\Delta}_f(t)$, contained in Eq. (15), and the Bloch energy ε_i, given by Eq. (4). In order to accelerate the convergence of the numerical integration over $\vec{K}$, in the sum of Eq. (15) we have introduced the factor $\zeta(\vec{R})=\exp[-\kappa(|X|+|Y|)]$, which takes into account the region of the sample that is effectively affected by the laser pulse, with κ being related to the lighted region in the surface plane. In this way, the function $S_f(t)$ is expressed as $S_f(t)=\sum_{\vec{R}}\exp[i\vec{\Delta}_f(t)\cdot\vec{R}]\ \zeta(\vec{R})$, which presents a closed expression for a fcc lattice, like the one considered here. In our calculations the parameter κ was fixed as $\kappa = 0.001$ a.u., which is equivalent to including approximately 2000 crystal sites on the surface plane, and no variations were found by increasing this number.

First, we oriented the external field $\vec{F}(t)$ along the $\langle 100\rangle$ crystallographic direction, which was chosen as the $\hat{x}$ axis. Energy and azimuthal angular distributions of electrons emitted with a glancing angle with respect to the surface plane ($\theta_e = 3$ deg) are plotted in Figs. 1–3 for different few-cycle laser pulses, with ϕ being the azimuthal angle measured with respect to the field direction ($\hat{x}$ axis). In these figures contributions from the different initial bands -$F^-(2s)$, $F^-(2p0)$, and $F^-(2p1)$- are displayed separately. In order to investigate the effects produced by the crystal arrangement, in all the cases surface electron distributions are compared with spectra corresponding to the atomic case, where only one fluor anion is considered as target.

As the electric field was chosen parallel to the surface, the component of the momentum transfer perpendicular to the surface plane becomes independent of the time, giving rise to the same perpendicular factor -$S_{fz}=\sum_j\exp[i\Delta_{fz}Z_j]$, with Z_j the $\hat{z}-$ positions of the different atomic planes- in both terms of Eq. (13). Then the different atomic layers do not produce interferences at the level of the CSV transition amplitude, as given by Eq. (13). This shows that double-differential electron distributions coming from different atomic planes can be incoherently added, all of them displaying similar angular patterns, as it was numerically verified for the particular case of Fig. 1. Furthermore, for glancing ejection angles, as the one considered here, electrons ionized from internal layers travel a long distance through the material before being emitted to the vacuum, suffering energy losses due to multiple collisions in their outgoing paths [40]. This effect has not been included in our model, which describes the primary electron distribution only. Therefore, as a first estimation for grazing electron distributions, we can consider that primary emitted electrons are essentially ejected from the topmost atomic layer.

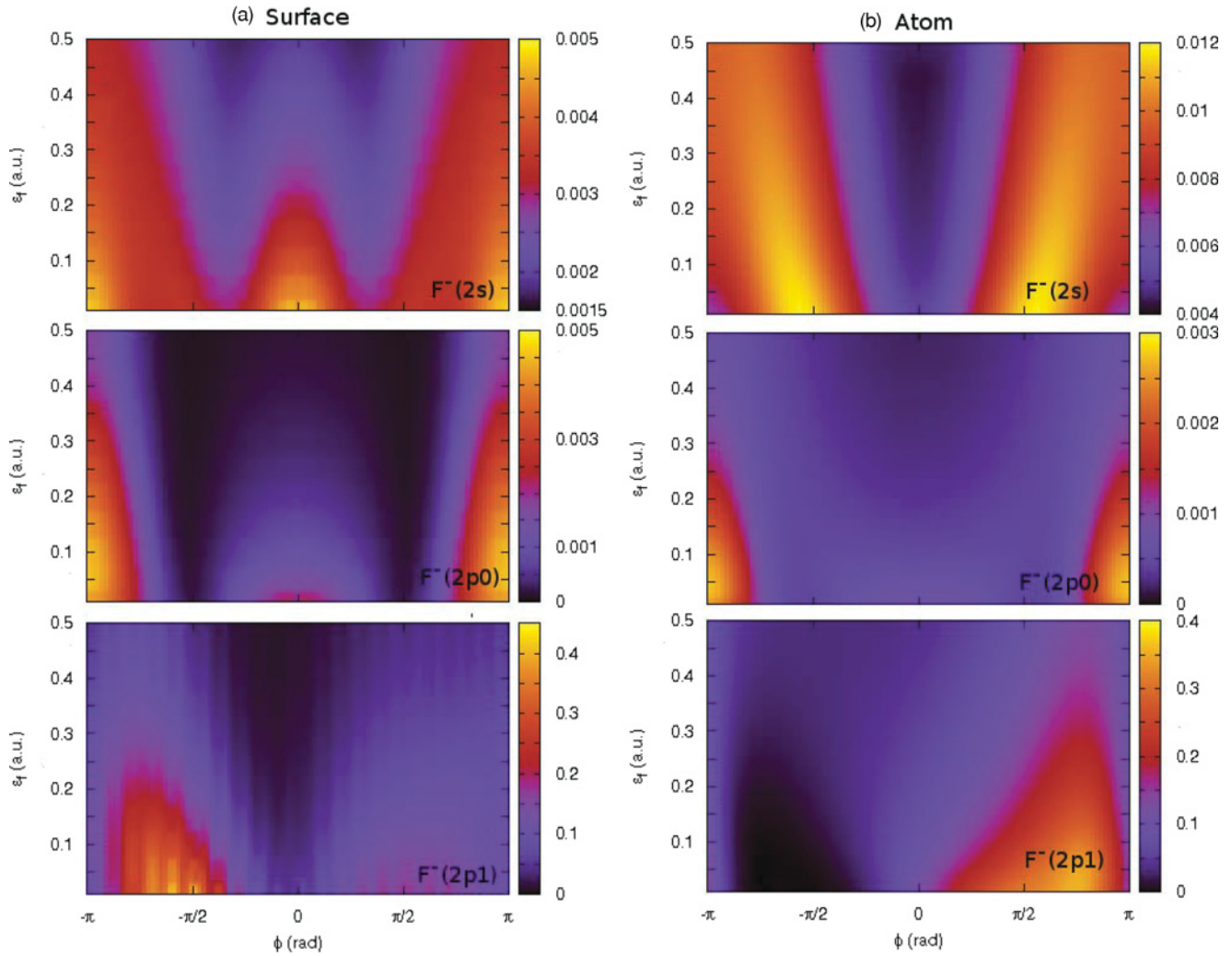

FIG. 1. (Color online) Angular and energy distributions for photoelectron emission from (a) a surface and (b) one F^- ion. The following initial surface bands are considered: $F^-(2s)$, $F^-(2p0)$, and $F^-(2p1)$. The parameters of the pulse are $F_0 = 0.01$ a.u., $w = 0.034$ a.u., and $\tau = 92$ a.u. (half-cycle pulse).

Figure 1 shows electron distributions produced by a half-cycle pulse with a carrier frequency $\omega = 0.034$ a.u., considering (a) the surface and (b) one F^- ion as targets. Electron emission spectra originating from the surface show modifications with respect to the atomic ones as a consequence of contributions of electrons that are ejected from different lattice sites. For the $F^-(2s)$ band, the electron emission probability from the crystal surface presents maxima in the forward and backward directions of the field, *i.e.*, at $\phi = 0$ and $\pm\pi$. While the preferential emission in the backward direction is associated with the classical movement of a free electron initially at rest, the increment of the electron emission in the field direction, just where the ejection from one F^- anion presents a minimum, is a consequence of the lattice interference produced by the presence of the function $S_f(t)$ in Eq. (13). The same happens for the $F^-(2p0)$ band, for which surface and atomic spectra display the main differences in the field direction. For the $F^-(2p1)$ band the emission from the surface tends to change the azimuthal asymmetry due to the initial atomic state, displaying a broad asymmetric maximum just around the region where the atomic spectrum displays a minimum. We found that this scenario does not change significantly as the duration of the pulse increases: similar structures are observed in surface electron distributions derived within the CSV approach when the number of cycles inside the envelope rises to three.

Within the present model, lattice effects essentially originate from the time dependence of $S_f(t)$, which shows that this function cannot be extracted as a common factor in Eq. (13). Therefore, the influence of the crystal on electron emission spectra is noticeable when the vector potential is comparable to or larger than the K radius of the Brillouin zone, K_B, as is the case for the laser parameters of Fig. 1. But when the maximum value of $A^-(t)$ inside the envelope, which is proportional to the ratio F_0/ω, is negligible with respect to K_B, effects produced by emission from the different lattice sites are blurred by the $\vec{K}$-integration. In Fig. 2 we plot surface and atomic electron distributions for a half-cycle pulse with a carrier frequency $\omega = 0.35$ a.u., that is, for a ratio F_0/ω ten times lower than that corresponding to Fig. 1. As expected, both surface and atomic spectra display similar shapes, with preferential emission in the backward direction of the field,

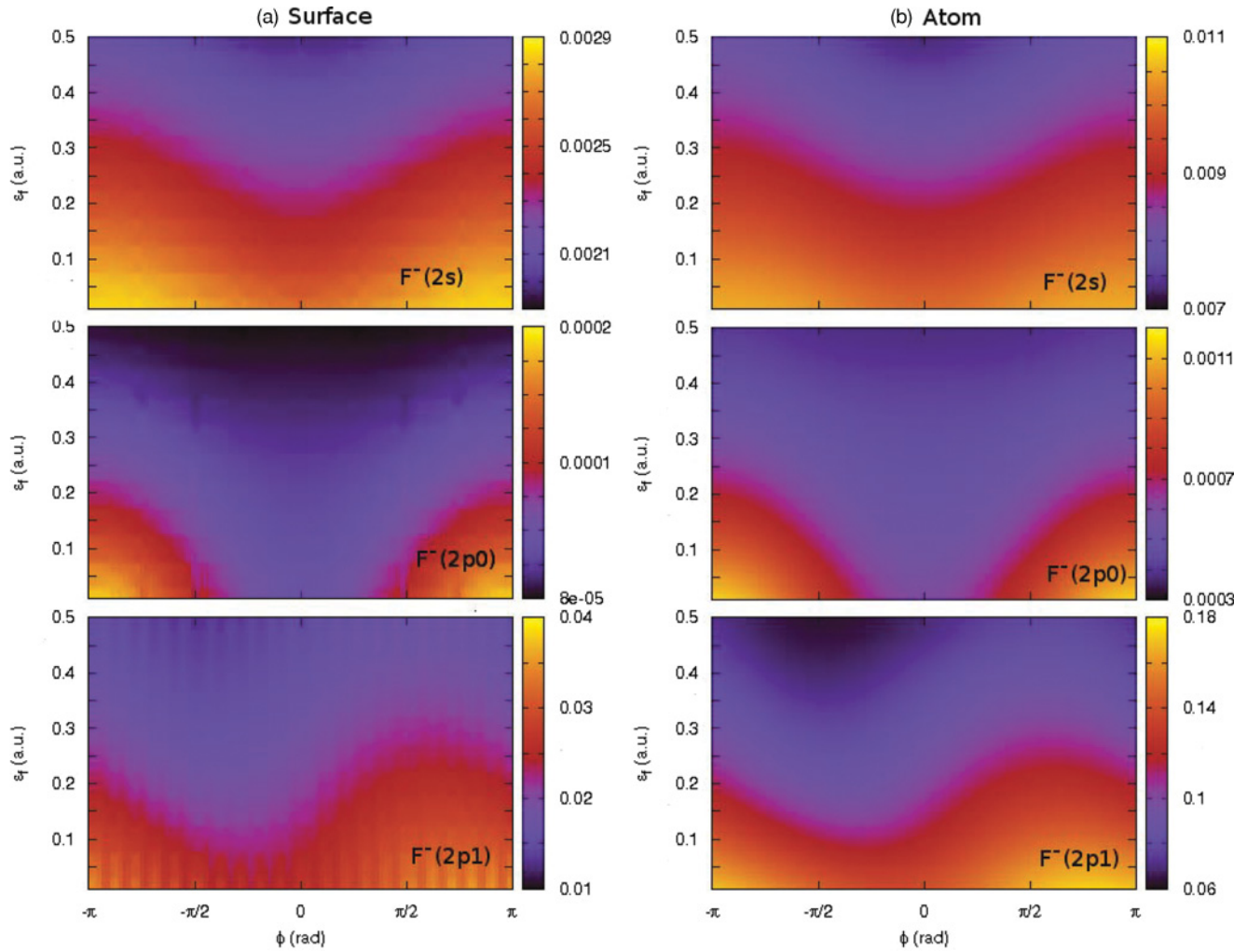

FIG. 2. (Color online) Similar to Fig. 1 for a laser pulse with $F_0 = 0.01$ a.u., $w = 0.35$ a.u., and $\tau = 9$ a.u. (half-cycle pulse).

in agreement with classical arguments. However, when the duration of the pulse increases to contain several oscillations of the electric field inside the envelope, weak surface effects arise in the electron distributions from the $F^-(2p)$ initial band, as observed in Fig. 3 for a three-cycle laser pulse. In this case, the structures of the atomic spectra are related to quantum interferences in time domain [41,42], which are affected by the ejection from different lattice sites for surface emission.

From Eq. (15), surface effects on the electron emission spectra are governed by the vector potential $\vec{A}^-(t)$. Hence, when the orientation of the field changes, the positions of the maxima of the angular spectrum rotate jointly with the vector potential, as shown in Fig. 4. Angular electron distributions produced by a field $\vec{F}(t)$ with a random orientation, which is rotated an angle $\phi_f = 1.92$ rad with respect to the $\hat{x}$ axis, present patterns that are just angularly shifted with respect those of Fig. 1. Notice that in the spectra of Fig. 4 there are no signatures of the crystal orientation, allowing us to conclude that the influence of the low-index crystallographic directions of the surface has been completely washed out by the $\vec{K}$ integration, something also observed for other coherent transitions from insulator surfaces [43].

Finally, to study the dependence of the surface spectra on the bandwidth δ_i, in Fig. 5 we plot the angular electron distributions of Fig. 1 for a given electron energy near the threshold ($\varepsilon_f = 0.01$ a.u.), comparing them with values obtained by fixing $\delta_i = 0$. We found a weak influence of the bandwidth, confirming that the observed surface effects are mainly due to the time dependence of the crystal factor $S_f(t)$. Notice that if the $\vec{K}$ dependence of the initial energy is completely neglected, the integral over $\vec{K}$ in Eq. (16) can be analytically solved, leading to an approximated expression for the differential emission probability from the surface band i,

$$\frac{dP_i}{d\varepsilon_f d\Omega_f} \approx \rho_e k_f \sum_{\vec{R}} |\mathcal{A}_{if}(\vec{R})|^2, \tag{17}$$

where every partial transition amplitude

$$\mathcal{A}_{if}(\vec{R}) = \left\langle \chi_f^{(at)-}(0) \middle| \varphi_i(0) \right\rangle - i \int_0^\tau dt\, e^{-i[\vec{A}^-(t)-\vec{A}^-(0)]\cdot\vec{R}} \times \left\langle \chi_f^{(at)-}(t) \middle| \mathcal{W}_f^\dagger(t) \middle| \varphi_i(t) \right\rangle \tag{18}$$

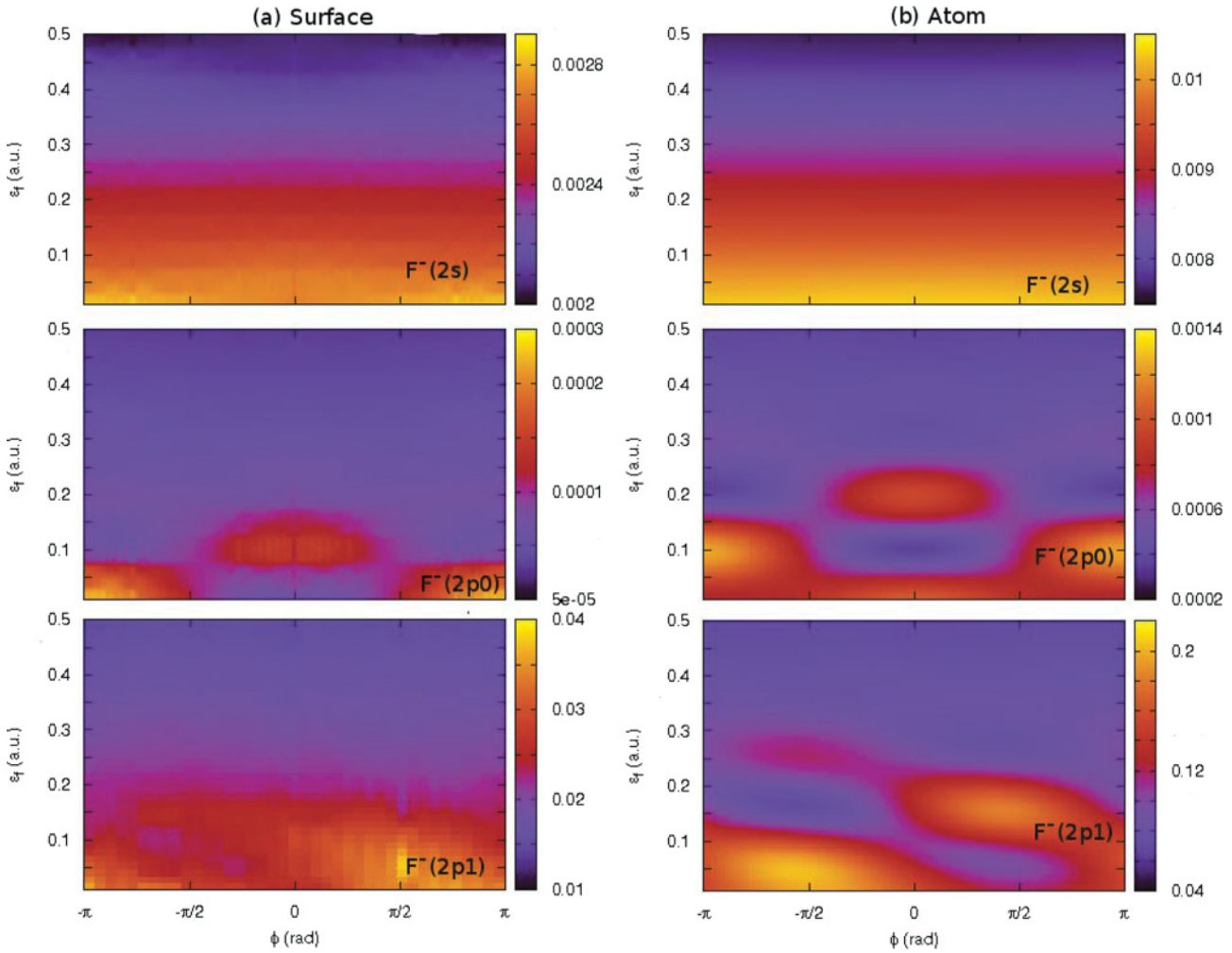

FIG. 3. (Color online) Similar to Fig. 1 for a laser pulse with $F_0 = 0.01$ a.u., $w = 0.35$ a.u., and $\tau = 54$ a.u. (three-cycle pulse).

includes a phase depending on the lattice site $\vec{R}$, given by the exponential factor in the integrand of the second term of Eq. (18). This time-dependent factor, not present in the atomic case, represents the main source of the crystal effects observed in the electron spectra of Fig. 4. On the other hand, even though the function $S_f(t)$ depends on the distance between

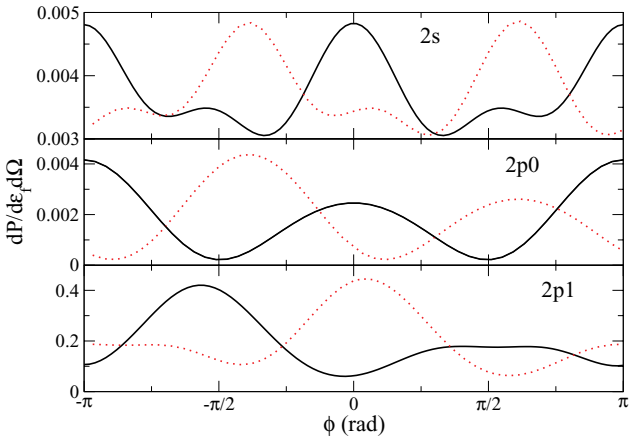

FIG. 4. (Color online) Angular electron emission spectra, corresponding to the electron energy $\varepsilon_f = 0.01$ a.u., for two different azimuthal orientations ϕ_f of the external field: (solid line) $\phi_f = 0$ and (dashed red line) $\phi_f = 1.92$ rad. The parameters of the pulse are the same as in Fig. 1.

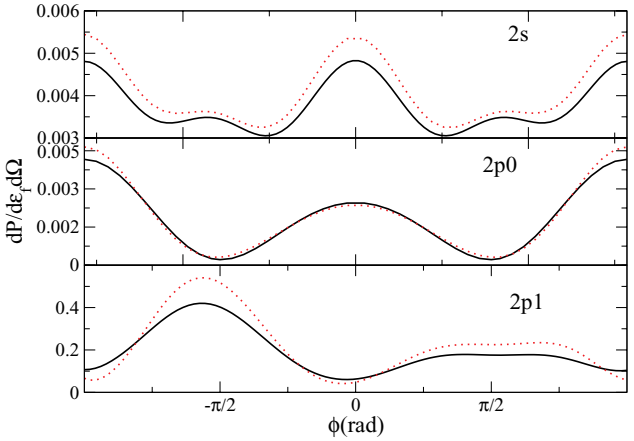

FIG. 5. (Color online) Angular electron emission spectra for the electron energy $\varepsilon_f = 0.01$ a.u.: (solid line) CSV results, including the bandwidth in the initial energy, as given by Eq. (4) and (dashed red line) fixing the bandwidth to zero. The parameters of the pulse are the same as in Fig. 1.

surface ions, the influence of thermal vibrations of the lattice was found negligible at normal temperatures.

IV. CONCLUSIONS

We have studied double-differential electron distributions produced by the incidence of ultrashort laser pulses on a LiF(001) surface. Photoelectron emission from the insulator surface has been described by means of the CSV approximation, which takes into account the main features of the process. We found that as the vector potential associated with the external field is comparable to or larger than the K radius of the Brillouin zone, surface electron spectra display effects associated with the addition of contributions coming from different lattice sites, but when the modulus of $\vec{A}^-$ decreases, becoming negligible with respect to K values contained in the first Brillouin zone, surface spectra show similar structures to those of the atomic case.

ACKNOWLEDGMENTS

This work was carried out with financial support from CONICET, UBACyT, and ANPCyT of Argentina.

[1] E. Goulielmakis, V. S. Yakovlev, A. L. Cavalieri, M. Uiberacker, V. Pervak, A. Apolonski, R. Kienberger, U. Kleineberg, and F. Krausz, Science **317**, 769 (2007).
[2] R. Kienberger *et al.*, Nature (London) **427**, 817 (2004).
[3] C. A. Haworth, L. E. Chipperfield, J. S. Robinson, P. L. Knight, J. P. Marangos, and J. W. G. Tisch, Nat. Phys. **3**, 52 (2007).
[4] A. Baltuska *et al.*, Nature (London) **421**, 611(2003).
[5] L. Miaja-Avila, C. Lei, M. Aeschlimann, J. L. Gland, M. M. Murnane, H. C. Kapteyn, and G. Saathoff, Phys. Rev. Lett. **97**, 113604 (2006).
[6] A. L. Cavalieri *et al.*, Nature (London) **449**, 1029 (2007).
[7] L. Miaja-Avila, J. Yin, S. Backus, G. Saathoff, M. Aeschlimann, M. M. Murnane, and H. C. Kapteyn, Phys. Rev. A **79**, 030901(R) (2009).
[8] A. K. Kazansky and P. M. Echenique, Phys. Rev. Lett. **102**, 177401 (2009).
[9] C. Lemell, B. Solleder, K. Tőkési, and J. Burgdörfer, Phys. Rev. A **79**, 062901 (2009).
[10] D. M. Volkov, Z. Phys. **94**, 250 (1935).
[11] F. H. M. Faisal, J. Z. Kamiński, and E. Saczuk, Phys. Rev. A. **72**, 023412 (2005).
[12] M. N. Faraggi, M. S. Gravielle, and D. M. Mitnik, Phys. Rev. A **76**, 012903 (2007).
[13] J. C. Baggesen and L. B. Madsen, Phys. Rev. A **78**, 032903 (2008).
[14] C.-H. Zhang and U. Thumm, Phys. Rev. Lett. **102**, 123601 (2009).
[15] N. W. Ashcroft and N. D. Mermin, *Solid State Physics* (Holt, Rinehart and Winston, New York, 1976), Chap. 10.
[16] A. Arnau, M. S. Gravielle, J. E. Miraglia, and V. H. Ponce, Phys. Rev. A **67**, 062902 (2003).
[17] K. Kimura, S. Usui, K. Maeda, and K. Nakajima, Nucl. Instrum. Methods Phys. Res. B **193**, 661 (2002).
[18] G. L. Yudin, S. Chelkowski, and D. Nandrauk, J. Phys. B **39**, L17 (2006).
[19] V. D. Rodríguez, P. Macri, and R. Gayet, J. Phys. B **38**, 2775 (2005).
[20] S. Selsto, J. F. McCann, M. Forre, J. P. Hansen, and L. B. Madsen, Phys. Rev. A **73**, 033407 (2006).
[21] H. R. Reiss, Phys. Rev. A **22**, 1786 (1980).
[22] P. A. Macri, J. E. Miraglia, and M. S. Gravielle, J. Opt. Soc. Am. B **20**, 1801 (2003).
[23] O. Smirnova, M. Spanner, and M. Isanov, J. Phys. B **39**, S307 (2006).
[24] G. L. Yudin, S. Patchkovskii, P. B. Corkum, and A. D. Bandrauk, J. Phys. B **40**, F93 (2007).
[25] D. G. Arbó, J. E. Miraglia, M. S. Gravielle, K. Schiessl, E. Persson, and J. Burgdorfe, Phys. Rev. A **77**, 013401 (2008).
[26] M. N. Faraggi, I. Aldazabal, M. S. Gravielle, A. Arnau, and V. M. Silkin, J. Opt. Soc. Am. B **26**, 2331 (2009).
[27] C.-H. Zhang and U. Thumm, Phys. Rev. A **80**, 032902 (2009).
[28] M. R. C. McDowell and J. P. Colleman, *Introduction to the Theory of Ion-Atom Collisions* (North-Holland, Amsterdam, 1970).
[29] J. E. Miraglia, J. Phys. B **15**, 4205 (1982).
[30] D. P. Dewangan and J. Eichler, Phys. Rep. **247**, 59 (1994).
[31] M. S. Gravielle and J. E. Miraglia, Nucl. Instrum. Methods B **258**, 21 (2007).
[32] G. Xiao, G. Schiwietz, P. L. Grande, N. Stolterfoht, A. Schmoldt, M. Grether, R. Kohrbruck, A. Spieler, and U. Stettner, Phys. Rev. Lett. **79**, 1821 (1997).
[33] G. R. Gomez, O. Grizzi, E. A. Sanchez, and V. H. Ponce, Phys. Rev. B **58**, 7403 (1998).
[34] L. Hägg, C. O. Reinhold, and J. Burgdörfer, Phys. Rev. A **55**, 2097 (1997).
[35] M. I. Stockman, M. F. Kling, U. Kleineberg, and F. Krausz, Nat. Photonics **1**, 539 (2007).
[36] G. Saathoff, L. Miaja-Avila, M. Aeschlimann, M. M. Murnane, and H. C. Kapteyn, Phys. Rev. A **77**, 022903 (2008).
[37] E. Clementi and C. Roetti, At. Data Nucl. Data Tables **14**, 177 (1974).
[38] Dz. Belkic, R. Gayet, and A. Salin, Phys. Rep. **56**, 279 (1979).
[39] A. Arnau (private communication).
[40] T. Boutboul, A. Akkerman, A. Breskin, and R. Chechik, J. Appl. Phys. **79**, 6714 (1996).
[41] S. Bivona, G. Bonanno, R. Burlon, D. Gurrera, and C. Leone, Phys. Rev. A **77**, 051404(R) (2008); S. Bivona, G. Bonanno, R. Burlon, and C. Leone, *ibid.* **79**, 035403 (2009).
[42] D. G. Arbó, K. L. Ishikawa, K. Schiessl, E. Persson, and J. Burgdörfer, Phys. Rev. A **81**, 021403(R) (2010).
[43] M. S. Gravielle and J. E. Miraglia, Phys. Rev. A **71**, 032901 (2005).